Dalton Transactions

PAPER

View Article Online
View Journal | View Issue

Cite this: *Dalton Trans.*, 2019, **48**, 6863

The coordination behavior of 2,3-bis(diphenylphosphino)maleic-*N*-phenylimide towards copper, silver, gold and palladium†

Yingxia Wang,[a,b] Andreas Eichhöfer,[a,b,c] Florian Weigend,[b] Dieter Fenske[a,b,c] and Olaf Fuhr *[a,b,c]

Received 19th December 2018,
Accepted 16th April 2019

DOI: 10.1039/c8dt05003a

rsc.li/dalton

The bidentate phosphine bis(diphenylphosphino)-*N*-phenyl-maleimide (**L1**) is used to synthesize a series of complexes from coinage metals and palladium. Some of them are mononuclear species where one metal atom is coordinated by two phosphine ligands. Three of these complexes have been investigated in detail because they contain the initial ligand in an anionic, radical form (**L1′**) *i.e.* [Cu(**L1L1′**)] (**1**), [Ag(**L1L1′**)] (**7**), [Pd(**L1′**)$_2$] (**11**). **L1′** in **1**, **7** and **11** shows significant differences in its bonding parameters compared to free or coordinating **L1**. By magnetic measurements the radical nature of these three compounds could be verified. Quantum chemical calculations prove the existence of either one (**1** and **7**) or two (**11**) unpaired electrons localized on the ligand. Furthermore these calculations can explain that **1** and **7** show an asymmetric structure in solid state where one can clearly differ **L1** from **L1′**.

Introduction

The bidentate phosphine 2,3-bis(diphenylphosphino)maleic anhydride (**L2**)[1,2] and its derivatives[3–5] (Fig. 1) represent a class of ligands with low redox potentials. These potential differ depending on the heteroatom in the five-membered ring (**L1**: −1.37 V, **L2** −1.17 V). As a result of this property some of their transition metal complexes show an electron transfer from the metal ion to low lying, unoccupied acceptor states of the ligands; *e.g.* [(**L2**)Co(CO)$_3$][6] and [(**L3**)Mn(CO)$_4$].[7] Assuming that cobalt and manganese would have the formal oxidation state 0 these compounds have 19 valence electrons (VE) located at the metal atoms. Indeed as a consequence of the redox properties of the phosphine ligands one electron is transferred from the metal atom onto **L2** or **L3**, respectively, leading to cobalt and manganese in oxidation state +I (18 VE) with the charge balanced by the resulting **L2**$^-$ or **L3**$^-$ radical anions.

Reactions of [Ni(CO)$_4$] or [M(PPh$_3$)$_4$] (M = Ni, Pd, Pt) with two equivalents of 2,3-bis(diphenylphosphino)-*N*-methyl-maleimide (**L3**) lead to complexes with the composition [M(**L3**)$_2$].[8] For M = Ni the metal atom is tetrahedrally coordinated and this compound is diamagnetic. Accordingly nickel has the oxidation state 0 and both ligands **L3** are neutral. In case of palladium and platinum paramagnetic compounds are formed showing square-planar coordination typical for Pd^{2+} and Pt^{2+} ions (d^8 configuration). Obviously two electrons of the metal atoms were transferred onto the two ligands. In this context these complexes can be described as [M^{2+}(**L3**$^-$)$_2$]. Similar electron transfer processes have also been described for various complexes containing so-called non-innocent ligands.[9–13] Examples for these ligands are indigo,[14] 2,2-azobispyridine,[15] iminoquinones,[16,17] phenanthroline,[18] *o*-iminosemiquinones[19,20] and *o*-iminobenzosemiquinonato.[21,22]

Another characteristic of this class of ligands is their tendency of undergoing various substitution and addition reactions in the coordination sphere of transition metals.[23–28]

[a]*Lehn Institute of Functional Materials (LIFM), Sun Yat-Sen University, 135 Xingang Road West, Guangzhou 510275, China*
[b]*Institut für Nanotechnologie (INT), Karlsruher Institut für Technologie (KIT), Hermann-von-Helmholtz-Platz 1, 76344 Eggenstein-Leopoldshafen, Germany*
[c]*Karlsruher Nano-Micro-Facility (KNMF), Karlsruher Institut für Technologie (KIT), Hermann-von-Helmholtz-Platz 1, 76344 Eggenstein-Leopoldshafen, Germany. E-mail: olaf.fuhr@kit.edu*

† Electronic supplementary information (ESI) available: Experimental details and crystallographic data. CCDC 1847908 (**L1**), 1847913–1847934 (**1a–13b**). For ESI and crystallographic data in CIF or other electronic format see DOI: 10.1039/c8dt05003a

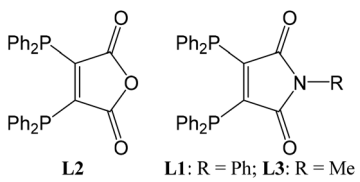

Fig. 1 Bis(diphenylphosphino)ligands on the basis of maleic anhydride.

In this article we report on the coordination behavior of **L1** with coinage metal ions and – in analogy to previous studies[8] – also palladium. Some of the new compounds were also investigated with respect to their magnetic properties and modeled by quantum chemical methods.

Results and discussion

Reactions of copper(I) acetate or silver cyclohexylthiolate with bis(diphenylphosphino)-*N*-phenyl-maleimide (**L1**) in boiling toluene lead to the formation of neutral mononuclear complex [M(**L1L1′**)] (M = Cu: **1**; Ag: **7**). These unexpected results can be explained by redox processes taking place at high temperatures: In case of **1** the initial copper(I) acetate is partly oxidized to copper(II) acetate whereas part of **L1** is reduced. The driving force for the formation of **7** might be the oxidation of the cyclohexylthiolate anions to dicyclohexyldisulfide.

An analogous gold compound could not be synthesized yet. The two compounds **1** and **7** show similar molecular structures (Fig. 2) where one metal atom is surrounded by the four phosphorus atoms of two ligand molecules in a distorted tetrahedral coordination sphere.

As stable compounds with copper or silver in oxidation state 0 have not been confirmed yet (and most probably do not exist),‡ we can surely assume that the metal atoms in **1** and **7** are in oxidation state +I. This indicates that one of the ligands has been reduced to the radical mono-anion **L1′**, which could be described by the resonance formulae shown in Fig. 3.

For comparison several more copper, silver and also gold complexes with **L1** were synthesized, in which the ligand remains in its neutral state. With copper(I) acetate the tetranuclear compound $[(CuOAc)_4(\mathbf{L1})_2]$ (**2**, Fig. 4, top) is formed. This compound consist of two $\{Cu_2(OAc)_2\mathbf{L1}\}$ subunits which dimerize by additional coordination *via* one of the oxygen atoms of one acetate of each subunit. Copper(I) halides yield the binuclear complexes $[Cu_2X_2(\mathbf{L1})_2]$ (X = Br^-: **3**; X = I^-: **3**, Fig. 4, middle) with a Cu_2X_2 four-membered ring and each **L1** ligand chelating one copper ion. In case of copper(II) sulphate a mononuclear dicationic complex $[Cu^{II}(\mathbf{L1})_2](SO_4)$ (**5**, Fig. 4, bottom) is formed where the $[Cu^{II}(\mathbf{L1})_2]^{2+}$ dication consists of a copper(II) ion coordinated by two neutral **L1** ligands very similar to the structure of the neutral compound **1**.

Additionally we performed a reaction analogous to the formation of **1** offering a 1 : 1 mixture of the ligands **L1** and 2,3-bis(diphenylphosphino)maleic anhydride (**L2**) where we could isolate a neutral mononuclear complex [Cu(**L1L2′**)] (**6**, Fig. 5). As in **1** this compound shows a copper atom which is coordinated by the four phosphorus atoms of the two ligands in a highly distorted tetrahedral arrangement.

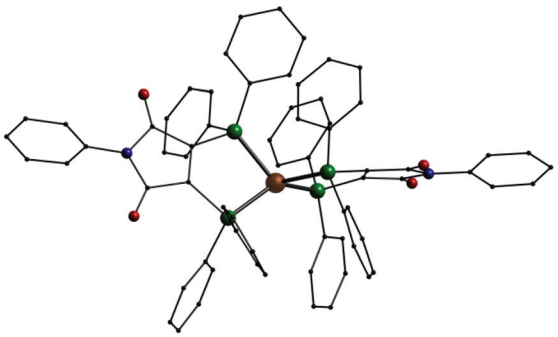

Fig. 2 Molecular structure of **1** in solid state; Cu: copper, P: green O: red, N: blue, C: black, H atoms omitted.

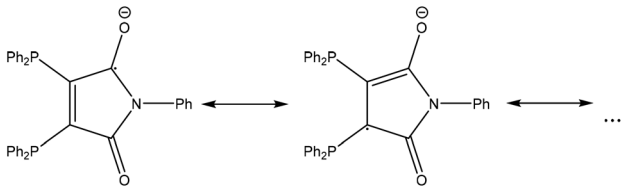

Fig. 3 Resonance formulae of the radical mono-anion $\{(Ph_2P)_2(C_4O_2N)Ph\}^{\bullet-}$ (**L1′**).

Using silver nitrate the reaction with pure **L1** yields another cationic mononuclear complex, $[Ag(\mathbf{L1})_2]NO_3$ (**8**). Analogous complexes could also be synthesised from gold(I) sources: $[Au(\mathbf{L1})_2]X$ (X = Cl^-: **9**; X = PF_6^-: **10**, Fig. 6). In these three compounds the cations once more consist of a metal(I) ion tetrahedrally coordinated by the phosphorus atom of two **L1** ligands. Just recently a digold complex $[(AuCl)_2\mathbf{L1}]$ was published, where the two gold(I) ions show the typical linear coordination.[29]

In addition we also investigated the coordination behavior of palladium with **L1**. Starting from the palladium(0) compound $[Pd(Ph_3)_4]$ the neutral mononuclear complex $[Pd(\mathbf{L1}')_2]$ (**11**, Fig. 7, top) is formed. An analogous species (**A**) has been described in the past using $(Ph_2P)_2(C_4O_2N)Me$ (**L3**) as ligand.[7] In **11** the palladium atom is surrounded by the four phosphorus atoms in a square planar coordination sphere typical for palladium in oxidation state +II. This means that in **11** the two ligands are present in their reduced anionic form **L1′**. Once more we synthesized two compounds for comparison. Even with an excess of **L1** the reaction of $[PdCl_2(PPh_3)_2]$ only leads to an substitution of the PPh_3 ligands resulting in $[PdCl_2(\mathbf{L1})]$ (**12**, Fig. 7, middle). In the presence of KPF_6 the mononuclear complex $[Pd(\mathbf{L1})_2](PF_6)_2$ (**13**, Fig. 7, bottom) is formed. Also **12** and **13** show the typical square planar coordination of palladium(II) and once more the dication in **13** is very similar to the neutral compound **11**.

The free ligand **L1** as well as all metal complexes **1–13** could be isolated as crystalline materials and their structures

‡In the 1960s and 1980s few reports about copper(0) and silver(0) compounds[35–38] were published, but in more recent publications none of these compounds is mentioned any more (in one case even the original authors themselves doubt their previous report[39]). Standard textbooks of inorganic chemistry also do not note any stable copper(0) or silver(0) compounds.[40,41] Instable copper carbonyls have been detected captured in solid argon or neon matrix.[42,43]

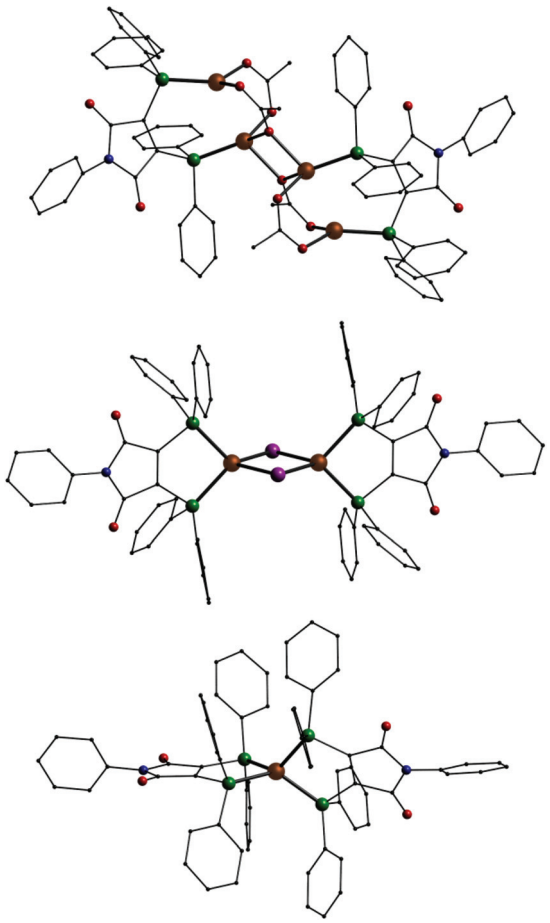

Fig. 4 Molecular structures of $[(CuOAc)_4(\mathbf{L1})_2]$ (**2**) (top), $[Cu_2I_2(\mathbf{L1})_2]$ (**4**) (middle) and the dication $[Cu^{II}(\mathbf{L1})_2]^{2+}$ in **5** (bottom); Cu: copper, P: green O: red, N: blue, C: black, I: violet, H atoms omitted.

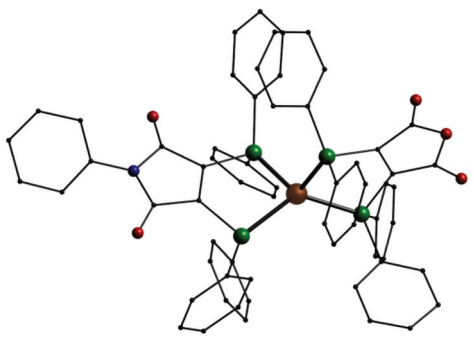

Fig. 5 Molecular structure of [Cu(**L1L2'**)] (**6**); Cu: copper, P: green O: red, N: blue, C: black, I: violet, H atoms omitted.

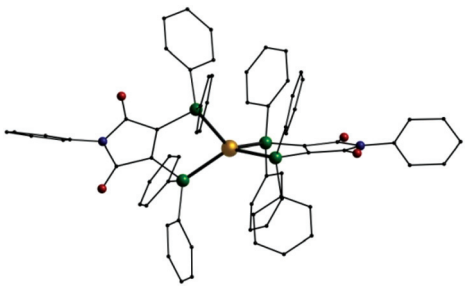

Fig. 6 Molecular structure of the monocation $[Au(\mathbf{L1})_2]^+$ in **10**; Au: gold, P: green O: red, N: blue, C: black, H atoms omitted.

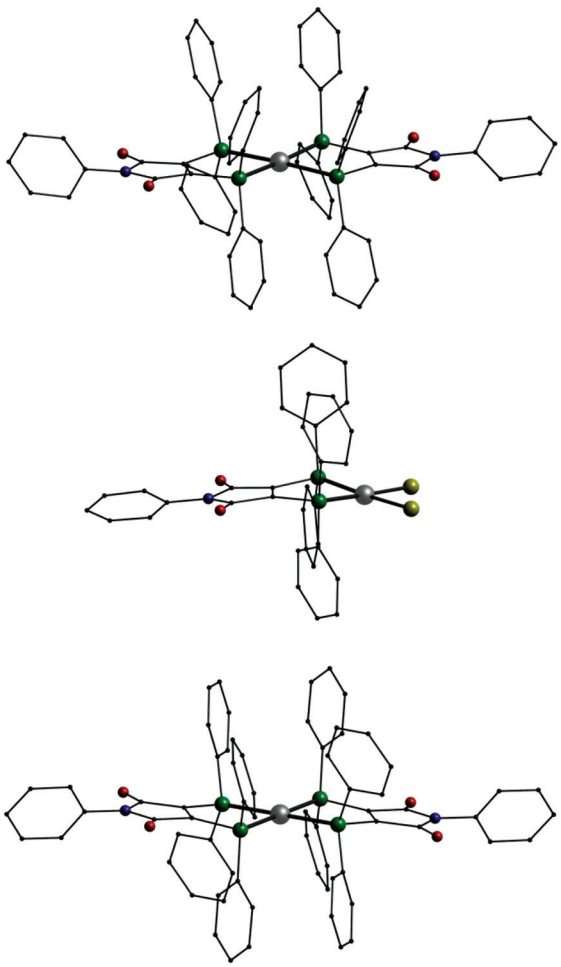

Fig. 7 Molecular structures of $[Pd(\mathbf{L1'})_2]$ (**11**, top), $[PdCl_2(\mathbf{L1})]$ (**12**, middle) and the dication $[Pd(\mathbf{L1})_2]^{2+}$ in **13** (bottom); Pd: grey, P: green, Cl: yellow, O: red, N: blue, C: black, H atoms omitted.

were determined by single crystal X-ray diffraction. In some cases the compounds crystallize in different packings mainly because of different amounts of incorporated solvent molecules. Compound **1** crystallizes in one reaction batch in two packing variations once in the orthorhombic space group $P2_12_12_1$ with the composition **1**·2toluene (**1a**) and secondly in the triclinic space group $P\bar{1}$ as **1**·toluene (**1b**). Also for **2** two different kinds of crystals are formed: monoclinic crystals in space group $P2_1$ having the composition **2**·DCM·$\frac{1}{2}$cyclohexane (**2a**, DCM = dichloromethane) and crystals in the triclinic space group $P1$ as **2**·2DCM (**2b**). Furthermore for **7** a monoclinic solvent-free version in space group $C2/c$ (**7a**) and a triclinic packing in space group $P1$ with one additional toluene mole-

cule (**7b**, with three molecules in the asymmetric unit) could be isolated. Species **9** can be crystallized in a triclinic version in $P\bar{1}$ as **9**·2toluene (**9a**) and monoclinic in $C2/c$ as **9**·3DCM (**9b**). Compound **10** always crystallizes from one reaction batch in two modifications: triclinic in $P\bar{1}$ (**10a**) and monoclinic in $P2_1/n$ (**10b**) both having the same composition **10**·$2\frac{1}{2}$DCM. Also for **11** two different kinds of crystals are yielded, one in the monoclinic space group $C2/c$ without additional solvent molecules (**11a**) the other one with one additional molecule of DCM in the space group Cc (**11b**). For **12** even three kinds of crystals were found, which grow simultaneously from one reaction batch: a trigonal form in space group $R3$ (**12a**), a monoclinic one in $P2_1/c$ (**12b**) and a triclinic form in $P\bar{1}$ (**12c**). Finally also **13** crystalizes as two different solvent adducts: **13**·2acetone (**13a**) and **13**·3DCM (**13b**). Detailed crystallographic and refinement data of **L1** and **1–13** are given in the electronic supplement in Table S1.†

One hint, that ligand **L1** got reduced in some reactions, are the bond lengths in the maleic imid part. Selected bond lengths of **L1** and **1–13** according to Fig. 8 are summarized in Table 1.

As highlighted by bold italic numbers in Table 1 in some of these compounds the bond lengths of the ligands differ significantly from those found in the free ligand. In agreement with the resonance formulae shown in Fig. 3 the C^B–C^B bonds are longer, the C^B–C^A bonds are shorter and the C^A–O bonds are longer compared to those in **L1**. Also the bonds C^B–P (shortened) and C^A–N (elongated) undergo changes in their lengths. Looking at the data for **1a** and **1b** the bond lengths suggest that in **1a** the complexes [Cu(**L1L1′**)] (**1**) are ordered in the packing with defined positions for **L1** and **L1′**. In contrast the bond lengths in **1b** are between those of pure **L1** and **L1′** indicating that the ligands are disordered while one can still assume that each complex should be neutral with composition [Cu(**L1L1′**)]. The same phenomena is found for **7a** and **7b**, both containing the neutral complex [Ag(**L1L1′**)]. For **7b** the two ligands have significantly different bond lengths indicating an ordered packing with precise positions for **L1** and **L1′**. On the other hand in **7a** the [Ag(**L1L1′**)] complex is located on a 2-fold axis (the refined asymmetric unit consists of half a molecule) and the bond lengths in the ligand are once more an average between **L1** and **L1′**. In case of the palladium complexes in **11a** and **11b** the distances clearly show that both ligands have been reduced and **11** should be formulated as a palladium(II) dication coordinated by two anionic **L1′** ligands.

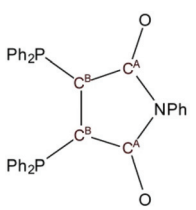

Fig. 8 Scheme of **L1** showing the atom labelling with respect to Table 1.

Compound **6** crystallizes with three molecules in the asymmetric unit. In case of this mixed complex where two different ligands are present the bond lengths indicate that **L1** is present in its neutral form whereas **L2** has been reduced to the analogous anion **L2′**.

For all other complexes – the copper compounds **2–5**, the silver species **8**, the gold complexes **9** and **10** § as well as the palladium compounds **12** and **13** – the bond lengths indicate that the ligands are present in their original non-charged state and also the oxidation states of the metal ions did not change. This is also in agreement with the anions which are present in these compounds. On the other hand no counterions were found in **1**, **7** and **11** during the refinement of the X-ray data leading to the statement that these complexes must be neutral.

Another method to verify the thesis that in some cases **L1** has been reduced is to look at the significant C–O vibrations in the IR spectra. The wavenumbers of the C–O vibration bands in IR spectra of **L1**, **L2** and **1–13** are summarized in Table 2.

The pure ligand **L1** shows one strong signal at 1711 cm^{-1} and a weak at 1767 cm^{-1}. For those compounds, where we assume the presence of the anionic ligand **L1′**, *i.e.* **1**, **7**, and **11**, additional bands between 1670 cm^{-1} and 1600 cm^{-1} are present whereas the other complexes show only the strong band between 1713 cm^{-1} and 1725 cm^{-1} and the weak one close to 1767 cm^{-1}. For the mixed species **6**, where we should also have one anionic ligand, three vibration signals are detected.

As the pure ligand **L1** is intensively orange in colour and **L2** is yellow, all compounds **1–13** are also coloured. The colours of **L1**, **L2** and **1–13** are listed in Table 3; absorption spectra of solid samples of these compounds in the UV-VIS-NIR range are shown in the supplement (Fig. S1–S13†).

Especially compounds **1**, **6**, **7** and **11**, which we suppose having ligands with unpaired electrons, are intensively dark in colour, a phenomenon typical for radicals. These effects can best be seen by comparing **7** with **8** or **11** with **13**, respectively. Looking at the structures of these pairs, the geometry and binding parameters of the complexes are very similar. In **7** and **8** there is one silver atom tetrahedrally surrounded by the four phosphorus atoms of the two ligands. Compound **7** – with the radical ligand **L1′** – is dark red, whereas **8** – with two neutral ligands **L1** and the charge being compensated by a nitrate anion – is bright orange. The same differences can be observed in the two palladium complexes, which both show a square planar coordination of the metal: the neutral compound **11** has a dark red to brown colour whereas the ionic compound **13** is yellow. These effects can also be seen in the solid state UV-VIS absorption spectra (Fig. 9) where the neutral compounds have significant absorption at higher wavelengths compared to the ionic ones. Looking at the spectra of **7** and **8**

§ All X-rayed crystals of **10a** and **10b** were found to be twinned. For **10a** only an uncomplete (87%) low quality data set could be obtained. This might be the reason for the large variations of the bond lengths for this compound compared to all other structures published in this paper.

Table 1 Selected bond lengths in **L1** and **1–13** in pm

Comp.	C^B–C^B	C^B–C^A	C^A–O	C^A–N	C^B–P
L1	134.8(2)	150.5(2), 151.3(2)	120.2(2), 120.3(2)	140.0(2), 140.1(2)	182.0(2), 183.3(2)
1a	133.4(8), ***139.9(9)***	***144.7(9), 145.4(9)***, 150.1 (9), 150.6(9)	120.1(8), 120.6(8), ***122.2 (8), 122.8(8)***	140.4(8), 141.7(8), ***142.2 (8), 142.3(8)***	***177.4(7), 178.0(6)***, 183.1 (6), 183.3(7)
1b	136.6(5), 138.2(4)	146.4(4), 146.5(5), 147.2 (4), 149.0(5)	121.3(4), 121.3(4), 122.0 (4), 122.1(4)	140.6(4), 140.7(5), 140.9 (4), 141.5(4)	180.2(3), 180.3(3), 180.5 (3), 180.7(3)
2a	134.2(2), 136.8(7)	149.3(9), 150.1(9), 151.3 (8), 153.8(9)	119.2(6), 120.1(6), 120.2 (7), 121.5(5)	138.5(7), 139.0(7), 139.0 (7), 140.6(7)	181.7(6), 182.8(6), 182.9 (6), 183.0(6)
2b	133.8(9), 134.5(9)	150.6(11), 151.1(11), 151.9 (12), 152.6(11)	118.2(9), 120.3(9), 120.5 (8), 121.1(8)	138.3(9), 139.9(8), 140.3 (11), 140.6(11),	182.4(7), 182.9(8), 184.5 (8), 184.7(8)
3	133.8(8)	151.2(7), 152.2(6)	119.1(8), 119.6(7)	139.3(8), 140.9(7)	181.2(5), 183.5(5)
4	133.7(5)	150.7(4), 151.1(4)	119.9(4), 120.2(4)	140.0(4), 140.3(4)	182.2(3), 182.9(3)
5	133.2(6), 134.7(6)	150.3(8), 150.8(7), 150.9 (6), 150.9(6)	119.7(5), 120.0(6), 120.2 (6), 120.4(7)	139.5(5), 139.9(6), 140.2 (7), 140.6(7)	181.4(4), 182.3(5), 182.5 (5), 182.7(4)
6 L1	133.4(5), 133.5(5), 134.1(6)	150.5(6), 151.3(5), 151.3 (6), 151.7(5), 152.3(7), 153.1(5)	119.2(6), 119.5(5), 119.8 (5), 119.9(6), 120.3(6), 120.8(5),	138.2(7), 138.5(6), 139.3 (5), 140.6(4), 140.7(5), 140.7(6)	180.8(4), 181.7(5), 182.3 (3), 182.5(4), 182.6(4), 182.7(4)
L2′	***139.9(5), 140.9(6), 141.4(7)***	***141.8(7), 142.1(5), 143.1 (5), 143.3(5), 144.7(5), 144.9(7)***	***120.7(5), 120.3(6), 121.8 (5), 121.8(7), 121.9(7), 122.4(5)***	***140.2(5), 140.5(5), 140.7 (5), 141.0(6), 141.1(7), 141.4(5)***	***177.3(5), 178.3(4), 178.6 (4), 178.8(4), 178.8(4), 179.1(5)***
7a	137.5(6)	146.6(7), 147.4(6)	121.5(6), 122.0(6)	140.8(5), 142.2(6)	180.0(5), 180.5(4)
7b	132.9(10), 133.0(10), 133.5(10), ***139.9(14), 142.1(13), 142.3(14)***	***141.7(11), 143.1(12), 144.0 (13), 144.8(10), 144.9(11), 145.2(15),*** 150.2(13), 150.7 (12), 151.3(13), 152.7(11), 153.8(13), 154.2(13)	117.9(9), 118.5(11), 119.5 (11), 119.8(9), 120.2(9), 120.9(10), ***121.9(11), 122.1 (10), 122.8(14), 123.9(10), 124.2(12), 124.6(12)***	138.8(10), 138.9(10), 139.0 (19), 139.1(11), 139.5(11), 140.4(10), ***140.5(10), 141.7 (11), 141.7(12), 142.0(12), 142.5(12), 142.7(12)***	***176.5(9), 177.3(8), 178.1 (8), 178.1(10), 178.4(9), 178.4(10)***, 181.5(9), 181.9 (9), 182.3(9), 182.8(8), 182.9(9), 182.9(10)
8	131.8(12), 134.7(13)	150.5(13), 150.6(14), 151.1 (15), 152.0(13)	119.4(12), 119.6(11), 119.8 (10), 120.3(11)	139.1(11), 139.1(11), 139.6 (12), 139.8(11)	181.8(10), 182.8(10), 184.1 (10), 184.1(10)
9a	134.5(12), 135.7(15)	149.5(14), 150.4(14), 151.8 (14),151.9(15)	119.7(14), 120.1(10), 120.5 (13), 120.7(11)	139.9(12), 140.5(14), 140.9 (15), 141.2(12)	180.2(12), 180.4(10), 180.6 (10), 182.0(9)
9b	132.5(9), 133.5(13)	150.7(10), 150.9(13), 151.5 (19), 151.4(11)	118.2(9), 118.8(12), 120.0 (10), 121.3(8)	136.4(9), 138.5(12), 141.7 (9), 142.2(9)	180.5(7), 182.4(8), 182.7 (7), 183.0(10)
10a	131.5(18), 138.8(17)	148.7(16), 149.9(16), 151.1 (14), 153.2(14)	118.8(16), 119.2(15), 124.8 (15), 128.6(17)	136.2(18), 136.3(15), 138.5 (16), 144.1(19)	177.4(12), 181.1(10), 181.4 (11), 182.9(13)
10b	132.7(12), 132.8(11)	150.4(9), 150.5(11), 152.8 (8), 153.2(9)	117.6(10), 119.(9), 120.9 (10), 121.0(10)	139.8(9), 141.3(10), 141.3 (10), 141.8(10)	181.0(7), 181.6(8), 181.9 (6), 183.0(6)
11a	***141.8(5)***	***143.2(7), 143.9(4)***	***122.1(3), 122.3(5)***	***143.4(6), 147.1(4)***	***175.9(3), 177.0(5)***
11b	***139.6(13), 141.1(10)***	***143.3(11), 143.4(11), 144.2 (12), 144.5(12)***	***122.2(10), 122.8(11), 123.3 (10), 123.4(10)***	***141.8(11), 141.8(11), 142.0 (10), 143.0(10)***	***175.4(7), 175.6(9), 176.1 (9), 176.2(9)***
12a	135.0(18)	149.0(14), 151.6(12)	118.4(14), 121.8(19)	137.9(17), 140(16)	179.6(10), 181.2(9)
12b	132.8(3), 132.8(3), 132.9(3), 133.0(3)	149.7(3), 149.7(3), 149.8 (3), 150.2(3), 150.2(3), 150.3(3), 150.6(3), 151.3(3)	119.3(3), 119.4(3), 119.8 (3), 119.9(3), 120.3(3), 120.4(3), 120.5(3), 120.7(3)	139.5(3), 139.8(3), 140.0 (3), 140.1(3), 140.6(3), 141.3(3), 141.7(3), 141.7(3)	181.6(2), 181.7(2), 181.8 (2), 181.9(2), 181.9(2), 182.0(2), 182.1(2), 182.3(2)
12c	132.0(13), 135.3(10)	149.6(14), 150.1(14), 150.5 (12), 151.7(15)	119.6(10), 119.7(9), 119.7 (9), 121.6 (12)	138.3(11), 141.2(13), 141.4 (10), 142.3(11)	181.0(10), 181.2(8), 181.7 (10), 183.4(11)
13a	132.9(5)	150.1(4), 150.9(4)	120.0(4), 120.3(5)	139.1(4), 139.1(5)	180.4(3), 180.5(3)
13b	132.8(4)	150.9(4), 151.0(4)	119.7(3), 119.9(3)	139.5(4), 139.7(3)	180.6(3), 181.0(3)

the absorption of **7** is red shifted (Fig. 9, top). Comparing **11** with **13**, (Fig. 9, bottom) the spectrum of compound **11** shows a broad absorption signal in the near IR region cantered at 930 nm.

Magnetic properties

The static magnetic behavior of complex [Cu(**L1L1′**)] (**1**) was studied between 2 and 300 K in a field of 1000 Oe (Fig. 10). At 2 K the value of χT (0.30 cm^3 mol^{-1} K) is below the one expected for a spin state of $S = 1/2$ with one unpaired electron localized on one of the ligands. With increasing temperature χT displays a small linear increase. In agreement with these observations the data could be fitted by the PHI program[30] (eqn (S1) in ESI†) with the parameters $S = 1/2$, $g = 1.79$ and a TIP of 4.4×10^{-4} cm^3 mol^{-1}. The simultaneous fit of the magnetization data (Fig. S14 in ESI†) taken at 2 K, 3 K, 4 K, 6 K, 10 K and 25 K display some slight deviations especially for the data at lower temperature and higher fields.

The static magnetic behavior of complex [Ag(**L1L1′**)] (**7**) was studied between 2 and 150 K in a field of 5000 Oe (Fig. 11). At 2 K the value of χT (0.36 cm^3 mol^{-1} K) is close to the one expected for a spin state of $S = 1/2$ with one unpaired electron localized on one of the ligands. With increasing temperature χT displays a small linear increase. In agreement with these observations the data could be fitted by the PHI program[30] (eqn (S1) in ESI†) with the parameters $S = 1/2$, $g = 1.953$ and a TIP of 4.27×10^{-4} cm^3 mol^{-1}. Above 150 K the paramagnetic signal of the sample continuously changes to a diamagnetic one due to the significant diamagnetic contribution of the two ligands ($\chi_{dia} = -910\ 10^{-6}$ cm^3 mol^{-1}) which causes centering problems and makes an evaluation of the data unreliable.

Table 2 Wavenumbers of the C–O vibration bands in IR spectra of **L1**, **L2** and **1–13** in cm^{-1}

Comp.	Wavenumber/cm^{-1}
L1	1767, 1711
L2	1762, 1716
1	1770, 1717, 1664, 1641, 1610
2	1767, 1713
3	1769, 1716
4	1769, 1716
5	1775, 1719
6	1718, 1649, 1602
7	1766, 1712, 1658, 1640, 1607
8	1773, 1716
9	1773, 1716
10	1775, 1719
11	1716, 1671, 1620
12	1774, 1719
13	1777, 1725

Table 3 Colours of **L1**, **L2** and **1–13**

Comp.	Colour
L1	Orange
L2	Yellow
1	*Dark reddish orange*
2	Bluish violet
3	Brownish blue
4	Bluish grey
5	Brownish red
6	*Dark orange*
7	*Dark red*
8	Orange
9	Red
10	Bluish violet
11	*Dark red to brown*
12	Yellow
13	Yellow

The static magnetic behavior of complex [Pd(**L1′**)$_2$] (**11**) was studied between 2 and 300 K in a field of 1000 Oe (Fig. 12). At room temperature the value of χT (0.68 cm^3 mol^{-1} K) is distinctly lower than the one expected for a spin state of S = 1 with two non-interacting unpaired electrons localized on each of the ligands. With decreasing temperature χT decreases down to a value of 0.44 cm^3 mol^{-1} K at 2 K indicative for an antiferromagnetic exchange interaction. In accordance, magnetization measurements at 2 K (Fig. S15 in ESI†) do not show saturation up to a field of 7 T with a maximum value of $M_H = 1.43 N_A \mu_B$ which is also well below a theoretical $M_S = 2$ for a spin state of S = 1.

Quantum chemical calculations

For two of the complexes (**1a** and **7b**) the two ligands of identical composition exhibit different structure parameters. One is apparently reduced while the other is not. This is unexpected, at least if considering a single molecule in the gas phase. One might rather have expected a partial reduction of both ligands, resulting from maximum delocalization of the unpaired electron. For clarification and quantification of the reasons for this symmetry breaking, quantum chemical calculations[31] were carried out with density functional techniques (B3-LYP functional,[32] polarized split-valence basis sets[33]). For model-

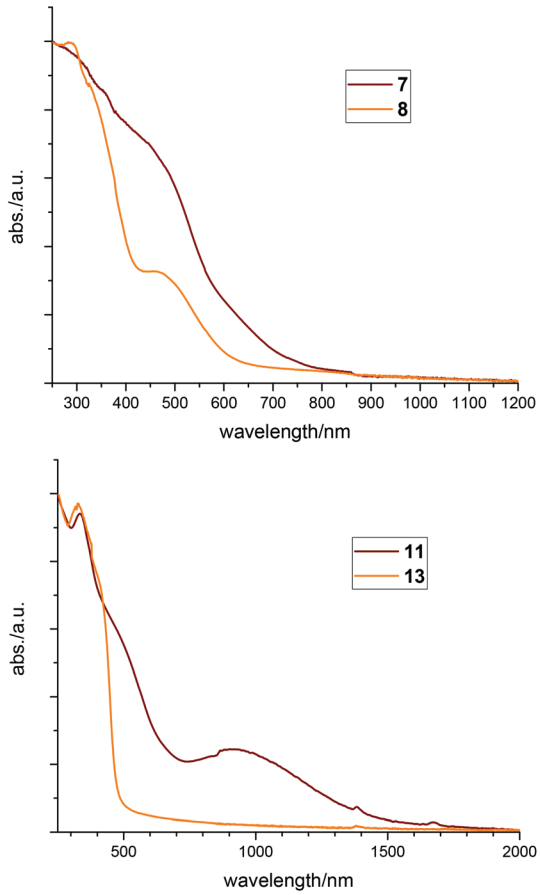

Fig. 9 Comparison of solid state UV-VIS spectra; top: **7** and **8**, bottom: **11** and **13**.

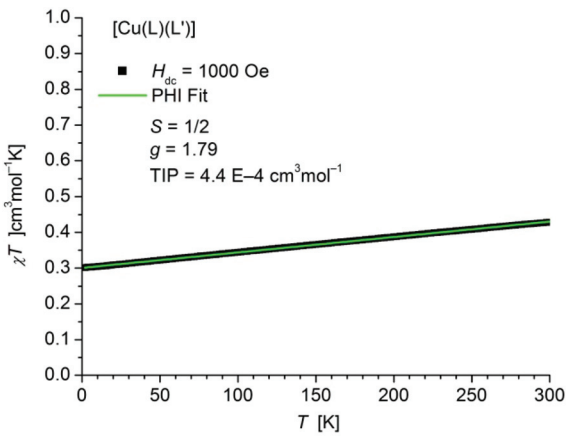

Fig. 10 Temperature dependence of χT of [Cu(**L1L1′**)] (**1**). The solid green line represents the result of the simultaneous fitting with the temperature dependent magnetization (Fig. S14 in ESI†) according to a Spin Hamiltonian (eqn (S1) in ESI†) by the PHI program.

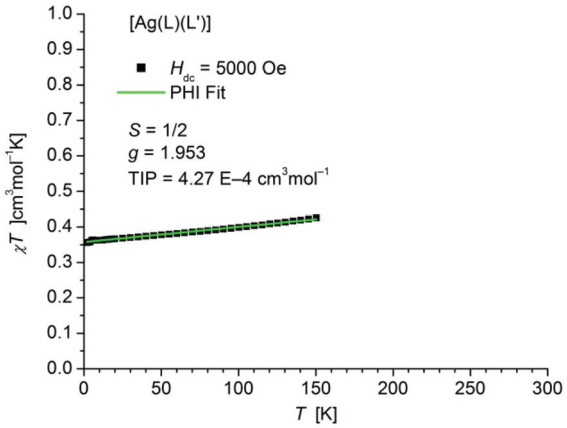

Fig. 11 Temperature dependence of χT of [Ag(**L1L1′**)] (**7**). The solid green line represents the result of the fitting according to a Spin Hamiltonian (eqn (S1) in ESI†) by the PHI program.

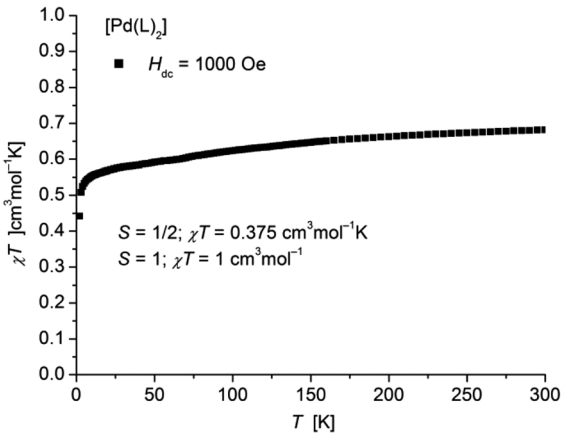

Fig. 12 Temperature dependence of χT of [Pd(**L1′**)$_2$] (**11**).

ling the electrostatic influence of neighbored molecules in the crystal the conductor-like screening model (COSMO)[34] was used in some of the calculations; if applied it is always explicitly noted.

We start with considering the free ligands **L1** and **L2**. Their LUMOs are shown in Fig. 13. They are anti-bonding with respect to the C_B–C_B bond and bonding with respect to the C_B–C_A bonds. Consequently, the latter are shortened upon reduction while the former are elongated. This effect is also found in the experimental solid state structures for **1a**, **6**, **7b** and **11** (see Table 1). The changes amount to *ca.* 6 pm in both cases, see also Fig. 13. Thus, for instance the C_B–C_B distances are convenient measures for the oxidation state both in experimentally obtained and in calculated structures.

Studies were continued with optimizations of structure parameters of [Cu(**L1L2′**)] (**6**), [Cu(**L1L1′**)] (**1**), [Ag(**L1L1′**)] (**7**), [Ag(**L1L1**)]$^+$ (cation in **8**), [Pd(**L1′**)$_2$] (**11**) and [Pd(**L1**)$_2$]$^{2+}$ (dication in **13**). We always started from the experimental structure and used COSMO in all cases. The resulting C_B–C_B and C_B–C_A distances are listed in Table 4 together with the number of unpaired electrons on both ligands, as resulting from a Mulliken population analysis. The shorter type of C_B–C_B distances amounts to *ca.* 135 pm, the longer type to *ca.* 142 pm, very similar to the measured data, 132 to 135 pm and 140 to 142 pm, and also to that for the free ligands in the respective oxidation state, see Fig. 13. In particular, the asymmetric shapes of **6**, **1a** and **7b** are preserved. The numbers of unpaired electrons at the ligands are well correlated to the C_B–C_B and C_B–C_A distances: the unpaired electron always fully resides on the ligand with the longer C_B–C_B distance and the shorter C_B–C_A distances.

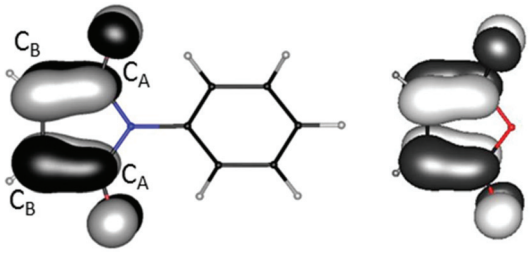

Fig. 13 Lowest unoccupied orbital of **L1** (left) and **L2** (right). The calculated C_B–C_B distances amount to 133.8/133.9/139.6/140.4 pm for **L1**/**L2**/**L1′**/**L2′**, the C_A–C_B distances to 150.2/149.5/143.3/143.2 pm. The vertical electron affinity was calculated to −0.72 eV for **L1** and to −0.84 eV for **L2**.

The asymmetric form of [Cu(**L1L2′**)] (**6**) – with **L2′** being reduced and incorporating the unpaired electron – is expected due to the higher absolute value of the electron affinity of **L2**, see Fig. 13. For [Cu(**L1L1′**)] (**1**) and [Ag(**L1L1′**)] (**7**) in contrast, the preservation of the asymmetric structure after its optimization (with COSMO) is a bit surprising. However, as exemplarily calculated for **1**, the energetic preference of the asymmetric structure (**A** as found in **1a**) over a symmetric structure (**S** in **1b**) amounts to 15 kJ mol^{-1}; **S** was obtained by interpolation between the two variants of **A** (Cu**L1L1′** and Cu**L1′L1**). We discuss this preference by comparing the total energy and the contribution from the interaction with the neighbored molecules in the crystal within COSMO, E_{int}, for three cases: structures **A**, and **S**, and a minimally distorted symmetric structure

Table 4 C_B–C_B and C_A–C_B distances for selected compounds optimized with B3LYP/def2-SV(P). Last two columns: Unpaired electrons at each of the ligands obtained with a Mulliken population analysis of the spin density

	d(C_B–C_B)/pm		d(C_A–C_B)/pm		Unpaired electr.	
	Left	Right	Left	Right	Left	Right
[Cu(**L1L2′**)] (**6**)	135.2	141.9	151.3; 151.6	144.1; 144.2	0	0.96
[Cu(**L1L1′**)] (**1**)	135.3	142.1	151.5; 151.7	145.1; 145.3	0	0.97
[Ag(**L1L1′**)] (**7**)	135.2	142.0	151.6; 151.7	145.3; 145.4	0	0.95
[Ag(**L1L1**)]$^+$ in **8**	135.2	135.1	151.7; 151.8	151.6; 151.7	0	0
[Pd(**L1′**)$_2$] (**11**)	140.6	140.7	146.4; 146.4	146.3; 146.4	0.92	0.94
[Pd(**L1**)$_2$]$^{2+}$ in **13**	135.1	135.2	151.5; 151.9	151.6; 151.9	0	0

S′ (derived from **S**), for which the two C_B–C_B distances differ by only 0.5 pm. For **S**, the singly occupied HOMO is the positive linear combination of the LUMO of **L1** at the right and **L1** at the left hand side of the molecule. The unpaired electron thus is equally distributed to the two ligands; for **S**, E_{int} amounts to 122 kJ mol^{-1}. For **S′** in contrast, the unpaired electron is located solely at the ligand with the slightly (0.5 pm) longer C_B–C_B distance. The resulting polarity of the molecule is energetically favorable for the interaction with the neighbor molecules: E_{int} increases by 25 kJ mol^{-1}. However, localization at only one of the ligands is unfavorable for the energy of the molecule itself. The total energy, which is the sum of the energy of the molecule and E_{int}, is worse for **S′** than for **S** by 4 kJ mol^{-1}. Thus, the energy gain by E_{int} obviously is (over) compensated by an energy loss due to the higher localization of the unpaired electron. Relaxation of the geometric structure of **S′** finally yields the antisymmetric structure **A**. This comes along with a gain in energy by 19 kJ mol^{-1} in the total energy. This gain is solely due to structure relaxation; the interaction energy with the neighbored molecules is almost constant (E_{int} changes by only 0.1 kJ mol^{-1}) and yields the overall preference of 15 kJ mol^{-1} of **A** over **S**. In contrast, the analogous calculation with the environment interaction being neglected (by switching off COSMO) yields a slight preference of 3.5 kJ mol^{-1} for the symmetric species; moreover, in this case **A** no longer is a minimum but converges to **S** when performing a structure optimization. The observed asymmetry thus is not a simple effect of crystal packing, but the result of a fragile balance of energy needed for localizing the electron at one side and energy gained by interaction with the neighbor molecules in the crystal. If the latter plus the energy gain by subsequent structure relaxation effects are larger than the former, the molecule is asymmetric despite two identical ligands.

Conclusions

Using bis(diphenylphosphino)-*N*-phenyl-maleimide (**L1**) in coordination chemistry of coinage metals or palladium, respectively, one can isolate neutral mononuclear complexes were the ligand is reduced to form the anionic monoradical **L1′**: [Cu(**L1L1′**)] (**1**), [Ag(**L1L1′**)] (**7**) and [Pd(**L1′**)$_2$] (**11**). These compounds and a series of comparable complexes in which the ligand did not accept an electron were characterized by single crystal X-ray analysis. The nature of the reduced ligand in **1**, **7** and **11** could be verified by several indicators: the bond lengths in **L1** and **L1′** show significant differences, the CO vibration signals in IR spectra are shifted and also magnetic measurements proved the existence of unpaired electrons. Also quantum chemical calculations show the presence of unpaired electrons localized on the ligands in compounds **1**, **6**, **7** and **11**. Furthermore calculations for **1** show a small but significant preference for the asymmetric arrangement, *i.e.* localization of the electron on one side of the complex, in contrast to symmetric arrangement with the electron being delocalized on both ligands.

Conflicts of interest

There are no conflicts to declare.

Acknowledgements

The authors are grateful to Mr Sven Stahl and Mrs Milena Staub for their assistance in the laboratory. This work was supported by the 111 project (90002-18011002) and the National Natural Science Foundation of China (21720102007).

Notes and references

1 D. Fenske and H. J. Becher, *Chem. Ber.*, 1974, **107**, 117–122.
2 H. J. Becher, W. Bensmann and D. Fenske, *Chem. Ber.*, 1977, **110**, 315–321.
3 D. Fenske and H. J. Becher, *Chem. Ber.*, 1975, **108**, 2115–2123.
4 D. Fenske and A. Christidis, *Angew. Chem.*, 1981, **93**, 113–115, (*Angew. Chem. Int. Ed.*, 1981, **20**, 129–131).
5 H. J. Becher, D. Fenske and M. Heymann, *Z. Anorg. Allg. Chem.*, 1981, **475**, 27–34.
6 D. Fenske, *Angew. Chem.*, 1976, **88**, 415, (*Angew. Chem. Int. Ed.*, 1976, **15**, 381–382).
7 D. Fenske, *Chem. Ber.*, 1979, **112**, 363–375.
8 W. Bensmann and D. Fenske, *Angew. Chem.*, 1979, **91**, 754–755, (*Angew. Chem. Int. Ed.*, 1979, **18**, 677–678).
9 W. Kaim and A. Paretzki, *Coord. Chem. Rev.*, 2017, **344**, 345–354.
10 S. Kuwata and T. Ikariya, *Chem. Commun.*, 2014, **50**, 14290–14300.
11 S. Sproules and K. Wieghardt, *Coord. Chem. Rev.*, 2010, **254**, 1358–1382.
12 A. B. P. Lever, *Coord. Chem. Rev.*, 2010, **254**, 1397–1405.
13 P. Deplano, L. Pilia, D. Espa, M. L. Mercuri and A. Serpe, *Coord. Chem. Rev.*, 2010, **254**, 1434–1447.
14 M. Chatterjee, P. Mondal, K. Beyer, A. Paretzki, W. Kaim and G. K. Lahiri, *Dalton Trans.*, 2017, **46**, 5091–5102.
15 B. Sarkar, S. Patra, J. Fiedler, R. B. Sunoj, D. Janardanan, G. K. Lahiri and W. Kaim, *J. Am. Chem. Soc.*, 2008, **130**, 3532–3542.
16 S. Bhattacharya, P. Gupta, F. Basuli and C. G. Pierpont, *Inorg. Chem.*, 2002, **41**, 5810–5816.
17 M. G. Chegerev, A. V. Piskunov, A. A. Starikova, S. P. Kubrin, G. K. Fukin, V. K. Cherkasov and G. A. Abakumov, *Eur. J. Inorg. Chem.*, 2018, 1087–1092.
18 M. Wang, T. Weyhermüller and K. Wieghardt, *Eur. J. Inorg. Chem.*, 2015, 3246–3254.
19 C. N. Verani, S. Gallert, E. Bill, T. Weyhermüller, K. Wieghardt and P. Chaudhuri, *Chem. Commun.*, 1999, 1747–1748.
20 J. Jacquet, E. Salanouve, M. Orio, H. Vezin, S. Blanchard, E. Derat, M. Desage-El Murr and L. Fensterbank, *Chem. Commun.*, 2014, **50**, 10394–10397.

21 P. Chaudhuri, C. N. Verani, E. Bill, E. Bothe, T. Weyhermüller and K. Wieghardt, *J. Am. Chem. Soc.*, 2001, **123**, 2213–2223.
22 X. Sun, H. Chun, K. Hildenbrand, E. Bothe, T. Weyhermüller, F. Neese and K. Wieghardt, *Inorg. Chem.*, 2002, **41**, 4295–4303.
23 W. Bensmann and D. Fenske, *Angew. Chem.*, 1978, **90**, 488–489, (*Angew. Chem. Int. Ed.*, 1978, **17**, 462–463).
24 K. Ejsmont, W. H. Watson, J. Liu and M. G. Richmond, *J. Chem. Crystallogr.*, 2003, **33**, 541–547.
25 W. H. Watson, S. G. Bodige, J. Liu and M. G. Richmond, *Struct. Chem.*, 2003, **14**, 369–375.
26 W. Yu, O. Fuhr and D. Fenske, *J. Cluster Sci.*, 2012, **23**, 753–766.
27 W. Yu, L. Guggolz, O. Fuhr, D. Fenske and S. Dehnen, *Dalton Trans.*, 2015, **44**, 9363–9366.
28 W. Yu, Y. Wang, O. Fuhr, D. Fenske and S. Dehnen, *Dalton Trans.*, 2018, **47**, 1032–1035.
29 R. Nyamwihura, L. Yang, V. N. Nesterov and M. G. Richmond, *J. Mol. Struct.*, 2017, **1129**, 188–194.
30 N. F. Chilton, R. P. Anderson, L. D. Turner, A. Soncini and K. S. Murray, *J. Comput. Chem.*, 2013, **34**, 1164–1175.
31 *TURBOMOLE V7.2, 2017, a development of University of Karlsruhe and. Forschungszentrum Karlsruhe GmbH*, 1989–2007, TURBOMOLE GmbH, since 2007.
32 C. Lee, W. Yang and R. G. Parr, *Phys. Rev. B*, 1988, **37**, 785–789.
33 F. Weigend and R. Ahlrichs, *Phys. Chem. Chem. Phys.*, 2005, **7**, 3297–3305.
34 A. Klamt and G. Schürmann, *J. Chem. Soc., Perkin Trans.*, 1993, **2**, 799–805.
35 G. W. Wattand and J. W. Dawes, *J Inorg. Nucl. Chem.*, 1960, **14**, 32–34.
36 A. J. Layton, R. S. Nyholm, G. A. Pneumaticakis and M. L. Tobe, *Nature*, 1967, **214**, 1109–1110.
37 T. Murugesan, P. R. Sarode, J. Gopalakrishnan and C. N. R. Rao, *J. Chem. Soc., Dalton Trans.*, 1980, 837–839.
38 J. A. Howard, B. Mile, J. R. Morton and K. F. Preston, *J. Phys. Chem.*, 1986, **90**, 2027–2029.
39 A. J. Layton, R. S. Nyholm, G. A. Pneumaticakis and M. L. Tobe, *Nature*, 1968, **218**, 950.
40 F. A. Cotton, G. Wilkinson, C. A. Murillo and M. Bochmann, *Advanced Inorganic Chemistry*, 6th edn, Wiley, New York, 1999, pp. 854, 1097.
41 A. F. Hollemann, E. Wiberg and N. Wiberg, *Anorganische Chemie, Band2*, de Gruyter, Berlin, 103th edn, 2017, p. 1693.
42 H. Huber, E. P. Kündig, M. Moskovits and G. A. Ozin, *J. Am. Chem. Soc.*, 1975, **97**, 2097–2106.
43 M. E. Alikhani and L. Manceron, *J. Mol. Spec.*, 2015, **310**, 32–38.